Computer Modeling in Engineering & Sciences

Tech Science Press

https://doi.org/10.32604/cmes.2026.082244

ARTICLE

Machine Learning-Based Modeling of Tensile Properties of Glass-Fiber-Reinforced Polymer Pipes under Accelerated Saltwater Aging Conditions

Cristina Roxana Popa[1], Maria Tănase[2,*], Gheorghe Brănoiu[3], Elena-Emilia Sirbu[4,5] and Cătălina Călin[4]

[1]Automatic Control Computers & Electronics Department, Petroleum-Gas University of Ploieşti, Ploiesti, Romania
[2]Mechanical Engineering Department, Petroleum-Gas University of Ploieşti, Ploiesti, Romania
[3]Petroleum Geology and Reservoir Engineering Department, Petroleum-Gas University of Ploieşti, Ploiesti, Romania
[4]Chemistry Department, Petroleum-Gas University of Ploieşti, Ploiesti, Romania
[5]National Institute for Research & Development in Chemistry and Petrochemistry ICECHIM, Bucharest, Romania

*Corresponding Author: Maria Tănase. Email: maria.tanase@upg-ploiesti.ro

Received: 22 March 2026; Accepted: 12 May 2026; Published: 30 June 2026

ABSTRACT: Glass-fiber-reinforced polymer (GFRP) pipes are increasingly used in aggressive environments due to their high corrosion resistance and favorable mechanical properties. However, long-term exposure to saline environments and elevated temperatures can lead to degradation of their structural performance. This study investigates the influence of accelerated saltwater aging on the tensile behavior and structural characteristics of GFRP pipes and proposes machine-learning-based predictive models for the ultimate tensile strength (UTS). Experimental specimens were immersed in a 3.5% NaCl solution under controlled temperature and exposure time conditions. Tensile testing revealed that the unexposed samples exhibited a maximum UTS of 79.63 MPa, while aged specimens showed a gradual reduction in strength, although more than 80% of the initial tensile strength was retained after 60 days of exposure. Statistical analysis indicated that temperature was the dominant factor, contributing 60.24% to the variation in UTS, followed by exposure time with 33.72%, with the regression model explaining 93.96% of the total variance ($R^2 = 0.9396$). X-ray diffraction analysis revealed a decrease in the degree of crystallinity from 20.49% in the reference sample to 15.05% in the most degraded specimen, corresponding to an approximate 26.5% reduction, which correlated with the observed decline in mechanical strength. Several machine learning approaches were evaluated, including Artificial Neural Networks (ANN), Exponential Gaussian Process Regression, and Boosted Trees. Among them, ANN provided the highest predictive accuracy, demonstrating strong agreement between predicted and experimental UTS values. The results confirm that hydrothermal aging significantly affects both the microstructural and mechanical properties of GFRP pipes, while machine learning models represent effective tools for predicting their long-term performance under aggressive environmental conditions.

KEYWORDS: Machine learning; GFRP; aging; saltwater; tensile properties; X-ray diffraction

1 Introduction

Fiber-reinforced polymer (FRP) composites have become widely used in structural, marine, and industrial applications due to their high specific strength, corrosion resistance, and favorable durability compared with traditional steel or iron materials [1–3]. Among these applications, FRP pipes are increasingly employed in aggressive environments such as offshore platforms, desalination plants, and chemical processing facilities,

where corrosion resistance and lightweight design are essential for long-term operational efficiency [4]. The superior mechanical performance and environmental resistance of FRP materials have made them attractive alternatives to steel pipelines, particularly in environments where exposure to moisture, salts, and chemicals can significantly accelerate corrosion processes in metallic structures [5]. However, despite their advantages, FRP composites remain susceptible to environmental degradation mechanisms that may affect their long-term mechanical behavior and structural reliability.

Environmental exposure, especially under hygrothermal and saline conditions, can lead to significant changes in the physical and mechanical properties of polymer composites [6–8]. Moisture diffusion into the polymer matrix can cause swelling, plasticization, and weakening of the fiber–matrix interface, ultimately resulting in reductions in stiffness, tensile strength, and overall mechanical performance [9]. The long-term exposure of FRP materials to aqueous environments may also induce microcracking, fiber debonding, and interfacial degradation, which progressively compromise the structural integrity of composite systems [10]. For composite pipes specifically, such degradation mechanisms can significantly affect load-bearing capacity and durability, particularly when the materials are exposed to seawater or saline environments for extended periods [11–15].

Numerous experimental investigations have explored the effects of aggressive environments on the mechanical properties of FRP composites. For example, Stamenović et al. [11] examined the influence of acidic and alkaline environments on the tensile behavior of glass–polyester composite pipes and reported notable reductions in tensile properties after prolonged exposure. Similarly, Liao et al. [16] investigated the thermal aging behavior of E-glass fiber reinforced epoxy pipes and demonstrated that elevated temperatures accelerate degradation processes, affecting both the matrix and the fiber–matrix interface.

Călin et al. [7] analyzed the effects of temperature and chemical environments on GFRP pipes by exposing specimens to salt water and alkaline solutions at 20°C and 50°C and the results showed that higher temperature and alkaline conditions accelerate degradation, increasing diffusion and reducing mechanical performance, with notable decreases in flexural and tensile strength, while temperature was identified as the main factor affecting the mechanical behavior.

A similar work performed by Tănase et al. [6] evaluates the circumferential mechanical properties of GFRP pipes using the split-disk method, focusing on the effects of aggressive environments. Hoop tensile strength, elastic modulus, and Poisson's ratio were determined after exposure to saltwater, and alkaline solutions at 20°C and 50°C. and it was found that environmental conditions significantly influence mechanical performance, with higher temperatures and alkaline environments accelerating degradation (the ultimate tensile strength decreased by up to 21%, while the elastic modulus decreased by up to 21%, indicating reduced stiffness and deformation resistance).

Other studies have confirmed that temperature significantly influences the aging kinetics of composite materials by increasing diffusion rates and accelerating chemical reactions within the polymer matrix [17]. As temperature increases, the rate of moisture absorption and chemical degradation processes also rises, which may lead to more rapid deterioration of mechanical performance.

The durability of FRP composites in marine or chemically aggressive environments has therefore become an important research topic. Investigations into environmental aging have shown that immersion in seawater or saline solutions can significantly affect the long-term behavior of glass-fiber-reinforced polymer systems [14,15]. Salt ions can penetrate the polymer matrix and influence the stability of the fiber–matrix interface, leading to reductions in mechanical strength and stiffness over time [17]. Similar observations were reported by dos Santos et al. [18], who demonstrated that exposure to saline solutions can alter the performance of polymer composites by modifying the matrix properties and weakening the reinforcement

interface. In addition, environmental exposure can involve combined effects of moisture, temperature, and chemical interactions, which makes predicting long-term performance particularly challenging [19].

To address these challenges, accelerated aging tests are frequently used to simulate long-term environmental exposure within a relatively short experimental period. Such tests involve exposing specimens to elevated temperatures or aggressive environments to accelerate degradation processes and evaluate long-term durability [13]. Accelerated aging approaches have been widely applied to FRP materials used in civil infrastructure and marine structures to estimate service life and performance degradation [20]. For instance, accelerated hydrothermal aging experiments have been used to evaluate the long-term durability of glass fibers and composite laminates by extrapolating degradation trends through Arrhenius-type models [21]. Similarly, accelerated testing methods have been employed to predict durability of FRP bars and reinforcement systems subjected to sustained loads and aggressive environments [22,23].

Several researchers have also developed models to estimate long-term mechanical property degradation of FRP materials under environmental exposure. Early approaches relied on empirical degradation laws and reliability-based models to estimate the service life of composite systems [24]. More recent research has incorporated predictive approaches that combine experimental observations with mathematical models to evaluate durability and long-term performance [25]. Other studies have proposed simplified predictive models for evaluating mechanical behavior of composite materials subjected to salt-fog environments or other aggressive conditions [26]. Additional durability studies have examined the influence of hygrothermal environments on FRP rods and bars, providing insights into the mechanisms responsible for mechanical property degradation [27–29].

Although these traditional modeling approaches have significantly contributed to the understanding of FRP durability, they often rely on simplified assumptions and may not fully capture the complex nonlinear relationships between environmental conditions, exposure time, and material properties. The degradation behavior of polymer composites involves multiple interacting mechanisms, including moisture diffusion, thermal aging, chemical reactions, and interfacial damage. As a result, conventional analytical models may have limited capability in predicting mechanical performance when multiple environmental variables are simultaneously involved.

In recent years, machine learning (ML) techniques have emerged as powerful tools for analyzing complex material behavior and predicting mechanical performance in composite systems. Machine learning algorithms can identify nonlinear relationships between input variables and target responses by learning from experimental datasets, making them particularly suitable for modeling material degradation processes [30]. These approaches allow researchers to develop predictive models that integrate multiple environmental parameters, material characteristics, and experimental conditions without requiring explicit formulation of the underlying physical mechanisms.

The application of machine learning in FRP research has grown rapidly in recent years. Alhusban et al. [31] highlighted the increasing use of artificial intelligence techniques for analyzing and predicting the performance of FRP structures in civil engineering applications. Similarly, Avevor et al. [32] reviewed the use of ML-based models for damage detection, fatigue prediction, and structural health monitoring in FRP-strengthened systems, emphasizing their ability to improve prediction accuracy and support intelligent structural management strategies. Machine learning approaches have also been applied to predict the bond performance of FRP reinforcement in marine composite structures, demonstrating the capability of data-driven models to capture complex relationships between material properties and environmental conditions [33].

Recent studies have further demonstrated the potential of combining experimental testing with machine learning models to predict degradation behavior of composite materials under environmental exposure. For example, Hasan et al. [34] developed predictive ML models to evaluate the degradation of FRP composites subjected to hygrothermal aging conditions. Similarly, Karimi and Yu [35] integrated experimental aging tests with machine learning techniques to correlate accelerated and natural aging of CFRP/aluminum adhesive joints under hygrothermal environments. These hybrid experimental–computational approaches enable more accurate predictions of long-term material performance while reducing the need for extensive long-duration experimental campaigns.

Furthermore, machine learning models have also been proposed for predicting long-term durability and service life of FRP and FRP-reinforced concrete structures. Ren and Wang [36] presented a comprehensive review highlighting the potential of ML algorithms in durability prediction of composite materials, particularly when large datasets and multiple environmental variables are involved. Such models can analyze degradation patterns and predict mechanical property evolution under various environmental conditions, making them valuable tools for durability assessment and structural design optimization.

Despite the increasing use of machine learning methods in composite material research, only a limited number of studies have specifically addressed the prediction of tensile behavior of FRP pipes exposed to saline environments under varying temperatures and exposure durations. Given the widespread use of FRP piping systems in marine and coastal infrastructure, there is a clear need for predictive frameworks capable of estimating the mechanical performance of these materials under realistic environmental conditions.

Therefore, the present study investigates the influence of saline environmental exposure and temperature on the tensile mechanical properties of FRP pipes. Experimental specimens were immersed in saltwater for exposure periods of 30, 45, and 60 days at temperatures of 20°C, 40°C, and 60°C in order to simulate accelerated environmental aging conditions. Following the exposure process, tensile tests were conducted to evaluate the resulting mechanical behavior of the specimens. Subsequently, machine learning models were developed using the experimental dataset to predict the tensile properties of FRP pipes as a function of environmental exposure parameters. By integrating experimental characterization with data-driven predictive modeling, this research aims to contribute to improved understanding of environmental degradation in FRP pipelines and provide reliable tools for predicting their mechanical performance and long-term durability in aggressive service environments.

2 Materials and Methods

2.1 Materials and Immersion Procedure

The specimens were prepared from a Glass-Fiber-Reinforced Epoxy (GRE) pipe with an inner diameter of 105.2 mm and a wall thickness of 5.5 mm. For each exposure condition, three specimens were fabricated to ensure the repeatability of the experimental results. The immersion environment consisted of a 3.5% NaCl (sodium chloride) solution, with a measured pH of 7.05, simulating a saline corrosive medium commonly encountered in practical applications.

The pH of the solution was measured at the beginning and end of the study period and a small variation was observed, which demonstrates that the solution was not acidified. It is worth noting that the pH of the solutions was around 7.

2.2 Design of Experiment

The Design of Experiments (DoE) was used to structure the experimental matrix, allowing the factors influencing the behavior of the GFRP material and their corresponding levels to be systematically organized.

A full factorial design, comprising nine experimental conditions, was implemented to evaluate the effects of temperature (20°C, 40°C, and 60°C) and exposure time (30/45/60 days). The testing conditions are summarized in Table 1.

Table 1: Experimental matrix of temperature and exposure time for accelerated aging conditions.

Exp. No.	Temperature [°C]	Exposure Time [Days]
1	20	30
2	20	45
3	20	60
4	40	30
5	40	45
6	40	60
7	60	30
8	60	45
9	60	60

2.3 Accelerated Aging of GFRP Samples

The GFRP samples were immersed in sealed glass containers containing salt water. To investigate the effect of temperature, the containers were maintained at three different levels, namely 20°C, 40°C, and 60°C.

2.4 X-Ray Diffraction (XRD)

The X-ray diffraction (XRD) analysis was performed using a D8 Advance diffractometer (Bruker-AXS, Karlsruhe, Germany) equipped with a θ–θ configuration and Bragg–Brentano geometry, employing Cu-Kα radiation (λ = 1.54 Å). The samples were analyzed over a 2θ range of 5°–70°. The operating conditions set in XRD Commander were 40 kV and 40 mA, while the scanning parameters included a step size of 0.1° and a scan speed of 0.1°/5 s. Qualitative phase identification was carried out using DIFFRAC.EVA v14 software in combination with the ICDD database.

The degree of crystallinity X_C from the XRD spectra was determined using equation [7]:

$$X_C = \frac{\sum A_C}{\sum A_C + \sum A_{am}} \tag{1}$$

where A_C is the fitted areas of the crystal phase, and A_{am} is the fitted areas of the amorphous phase.

Evaluating the precision of Rietveld structural analysis involves monitoring specific reliability factors, primarily the Goodness-of-Fit (GOF) and the Durbin-Watson (DW) statistic. The GOF index is calculated as the quotient of the weighted-profile R-factor (Rwp) to the expected R-factor (Rexp), with a theoretical floor of 1.0. For a structural model to be deemed statistically sound, GOF values should ideally remain below 1.5, though values up to 2.0 are often acceptable in practice. Complementing this, the DW index assesses the degree of serial correlation among the residual errors. In an optimal XRD refinement, the DW value should approach 2.0; deviations from this indicate systematic errors in the model. High-quality refinements with minimized GOF and stabilized DW indices are essential for accurately detecting subtle structural modifications.

2.5 Tensile Testing

The experimental tests were performed at room temperature using a Walter + Bai LF300 universal testing machine, shown in Fig. 1, at a constant strain rate of 3 mm/min. The machine was equipped with an extensometer with a gauge length of 25 mm to ensure accurate measurement of the elastic modulus.

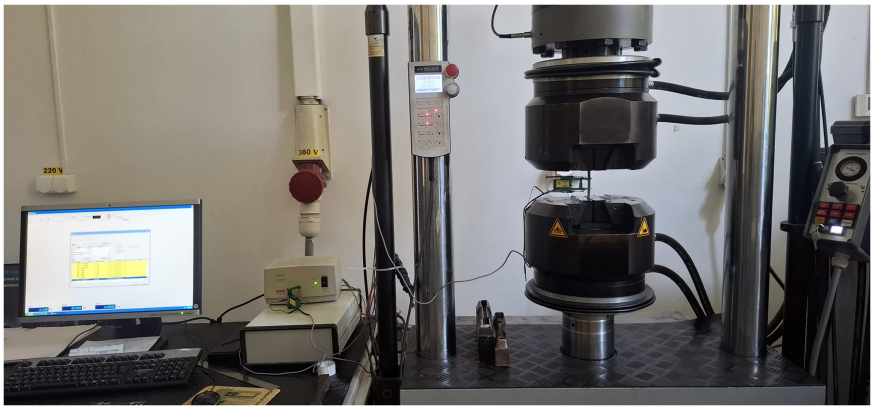

Figure 1: Tensile testing of GFRP samples.

3 Overview of Machine Learning

Machine learning (ML) is a field of artificial intelligence based on principles that allow systems to learn from data and make autonomous decisions without explicit programming [37,38]. Unlike traditional deterministic techniques, ML uses statistical models and adaptive algorithms capable of capturing complex relationships within data and subsequently generalizing to new information [39,40].

The following machine learning categories are distinguished in the literature [38]:

- Supervised learning, in this type of learning, the model receives input–output pairs from experimental data to learn functional dependencies [41,42]. These models include regression, feedback neural networks, support vector machine or boosting ensembles techniques [43].
- Unsupervised learning, in this case, the models analyze hidden structures in unlabeled data using methods such as clustering, principal component analysis, or density estimation [44].
- Reinforcement Learning—this type of learning trains an agent to interact with environment in such a way as to maximize a reward function and is commonly used in the optimization of autonomous control and resource management strategies [39].

Machine learning methods are particularly effective for modeling complex relationships that lack explicit analytical formulations. In this context, the durability of fiber-reinforced polymer (FRP) composite pipes can be evaluated with improved accuracy, as ML models can capture nonlinear relationships between stress–strain behavior and material degradation. This enables more reliable prediction of failure points and early identification of critical structural conditions, contributing to enhanced service life and structural health monitoring.

Recent studies highlight the increasing use of ML techniques for predicting the ultimate tensile strength (UTS) of FRP composite pipes. For example, Ang et al. [45] developed an artificial neural network (ANN) model that achieved approximately 90% prediction accuracy. Similarly, Mishra and Morisetty [46] compared several algorithms, including Decision Trees, Random Forest, XGBoost, CatBoost, and AdaBoost, and found that AdaBoost provided the best performance in terms of MSE, MAE, and R^2. In addition, Verma et al. [47]

reported superior predictive accuracy for ANN models compared to Gaussian Process Regression and Linear Regression.

In this study, a comparative analysis is conducted between classical polynomial regression and three supervised learning techniques for predicting the UTS of FRP composite pipes: Exponential Gaussian Process Regression (EGP), Boosted Trees (BT), and Artificial Neural Networks (ANN). All models were implemented using the Regression Learner toolbox available in the MATLAB environment.

Model performance was evaluated using standard statistical metrics, including the coefficient of determination (R^2), mean absolute error (MAE), root mean squared error (RMSE), and mean squared error (MSE). The mathematical definitions of these metrics are provided in [43].

3.1 Polynomial Regression

Polynomial regression (PR) is one of the classical analytical methods used for processing experimental data to determine the parameter values of mathematical models based on approximation relationships. The approximation function is represented by an n-th order polynomial that is shown in Eq. (2):

$$y_{output} = \sum_{i=1}^{n} a_i \cdot x^i \tag{2}$$

where (x_i, y_i), $i = \overline{1, n}$ denote the experimental data points.

The objective of the algorithm is to determine the coefficients a_i, $i = 1, \ldots, n$, by minimizing an objective function defined as the sum of squared errors between the experimental values and the predicted outputs, Eq. (3) [48]:

$$f(A) = \sum_{j=1}^{n} (y_i - \sum_{i=1}^{n} a_i \cdot x^i) \tag{3}$$

The polynomial regression model, although mathematically simple, was included as a baseline method and as a practical engineering tool. Its role is to provide a fast and straightforward approximation of the material behavior based on the available experimental data, without requiring complex training procedures. This approach enables a direct comparison with more advanced machine learning models, thereby highlighting the relative advantages and limitations of each method in terms of accuracy, complexity, and applicability.

3.2 Exponential Gaussian Process Regression

Exponential Gaussian Process Regression (EGP) is a machine learning technique that combines linear regression with exponential regression by employing a squared exponential kernel as its core function for modeling relationships between processed data. This approach results in correlations that decay exponentially with increasing distance between data points, enabling Gaussian Process Regression (GPR) to effectively interpolate the available data [49].

The interpolation relationship between the input–output data can be expressed by Eq. (4):

$$y = Ae^{-\frac{(x-\mu)^2}{2\sigma^2}} + \varepsilon \tag{4}$$

where x is the input data, y the output data, μ is mean (central Gaussian distribution), σ standard deviation, ε error.

3.3 Boosted Trees

Boosted Trees (BT) construct a predictive model by sequentially combining multiple decision trees. Each tree is trained to correct the errors made by the previous one through the minimization of a loss function, as described by Eq. (5) [50]:

$$y_{pred} = \sum_{i=1}^{m} \gamma_i \cdot h_i(x_i) \tag{5}$$

where γ_i denote the learning coefficient, m represents the number of trees, h_i is the i-th decision tree and x_i the input data.

3.4 Artificial Neural Networks

Artificial Neural Networks (ANN) represent adaptive machine learning models inspired by the information processing mechanisms of the human brain. They consist of interconnected computational units, referred to as artificial neurons, organized into an input layer, one or more hidden layers, and an output layer, through which information is propagated in a sequential manner. The network learns by iteratively adjusting the synaptic weights between neurons to minimize a predefined loss function, enabling the approximation of complex nonlinear relationships between input variables and output responses. As the training process progresses and the model is exposed to additional data, the predictive performance of the network is progressively improved. The equation of the function activation of ANN is shown Eq. (6) [45]:

$$y_{output} = \sum_{i=1}^{n} w_i \cdot I_i \tag{6}$$

where y_{output} the output value of each layer, w—weight of the neuron, I—weight of the neurons.

4 Results and Discussion

4.1 Tensile Testing Results

Fig. 2 shows the variation in ultimate tensile strength and strength retention of the GFRP specimens with exposure time and temperature. The unexposed specimens exhibited the highest tensile strength (79.63 MPa). After environmental exposure, a gradual decrease in tensile strength was observed as both temperature and exposure time increased. At 20°C, the reduction was moderate, while higher temperatures (40°C and 60°C) led to a more pronounced decrease in strength.

The variability of the experimental results was within ±7% of the mean values, indicating good repeatability of the measurements.

The strength retention results follow the same trend, decreasing from 0.92 (20°C, 30 days) to 0.83 (60°C, 60 days). These results indicate that elevated temperatures accelerate the degradation of GFRP, although the material retains more than 80% of its initial strength after 60 days of exposure.

A detailed analysis of the degradation mechanisms at the fiber–matrix interface for the same material system and identical saltwater immersion conditions has been previously reported by the authors in work [7]. In that study, scanning electron microscopy (SEM) revealed significant microstructural changes after exposure to saline environments, particularly at elevated temperatures. The formation of corrosion-related precipitates (orange–brown deposits) was observed on the surface of samples immersed at 50°C, indicating chemical interactions between the environment and the polymer matrix. Furthermore, SEM images highlighted clear differences between unexposed and aged specimens, showing that the polymer matrix undergoes surface exfoliation and localized degradation. These microstructural alterations indicate

weakening of the fiber–matrix interface and support the observed reduction in ultimate tensile strength in the present study.

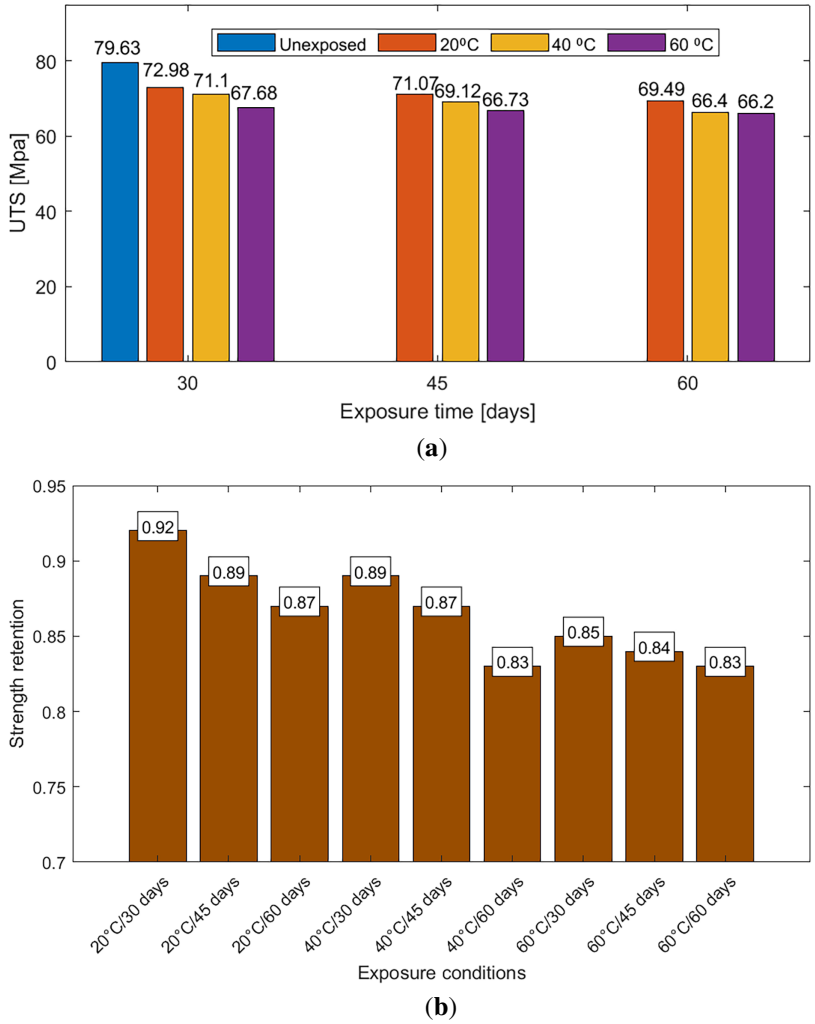

Figure 2: Tensile test results: (**a**) ultimate tensile strength; (**b**) strength retention.

4.2 XRD Results

The XRD spectra of GFRP samples (Fig. 3) exhibit a broad asymmetric halo in the range of 10°–25° (2θ), with a maximum around 18°, characteristic of the predominantly amorphous structure of the epoxy matrix and E-glass fibers [51]. In addition, diffraction peaks at 27.56°, 36.20°, 41.20°, 54.46°, and 56.54° are associated with microcrystalline silica phases originating from the glass fibers (ICDD-JCPDS 01-070-3755).

From a qualitative point of view, in the spectrum of the control sample R, the broad peak at 18° (2θ degrees) and a minor peak at 27.56° (011 plane) corresponding to the presence of microcrystalline silica fibers were recorded.

In the X-ray spectra of GFRPs (samples 1–9) a trend of decreasing intensity and broadening of the peak at 18° can be observed, suggesting a decrease in the degree of crystallinity of samples 1–9 (Fig. 3) correlated with the increase in temperature and exposure time to saline environments of the investigated samples. The broadening of the peaks and the decrease in the intensity of the peaks at 18° in the XRD spectra could be

associated with an increase in micro-tensions (micro-strain) at the GFRP surface caused by salt crystals penetrating and expanding the polymer structure [52–54].

The presence of other prominent peaks at 2ϑ degrees—27.56°, 36.20°, 41.20°, 54.46° and 56.54° in the X-ray spectra of the composite material (GFRP) samples 1–9 indicates that degradation of the polymer matrix and exposure in relief of the microcrystalline silica fiber, more resistant to degradation, occurred.

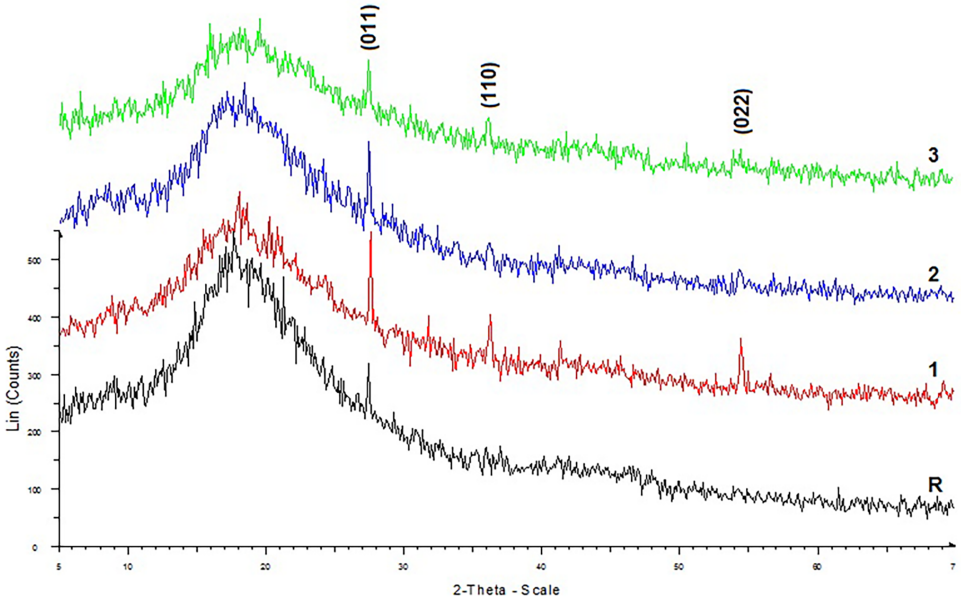

(**a**)

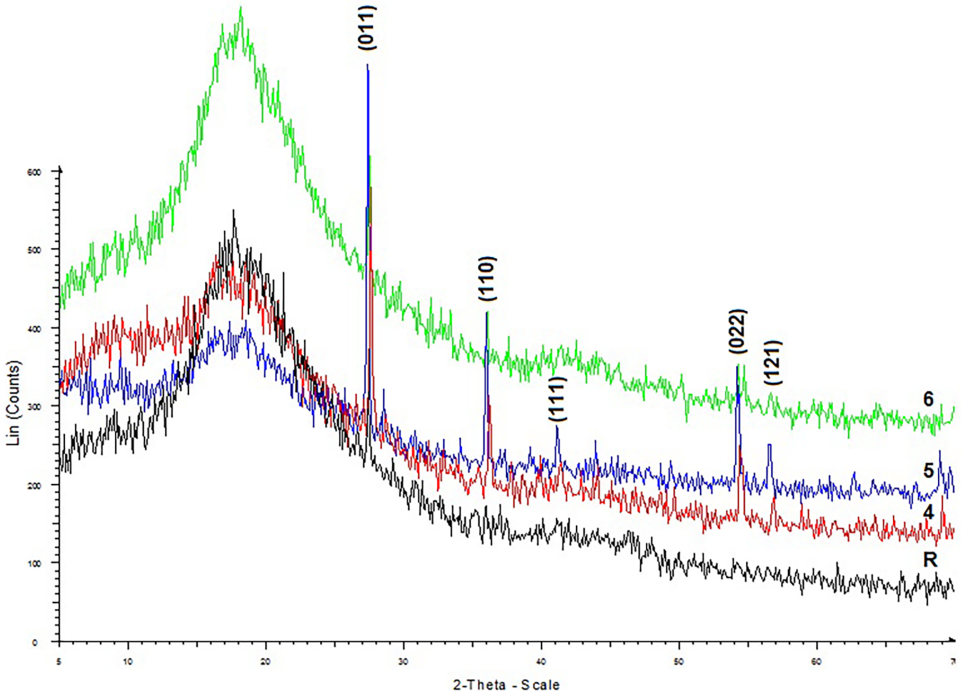

(**b**)

Figure 3: (Continued)

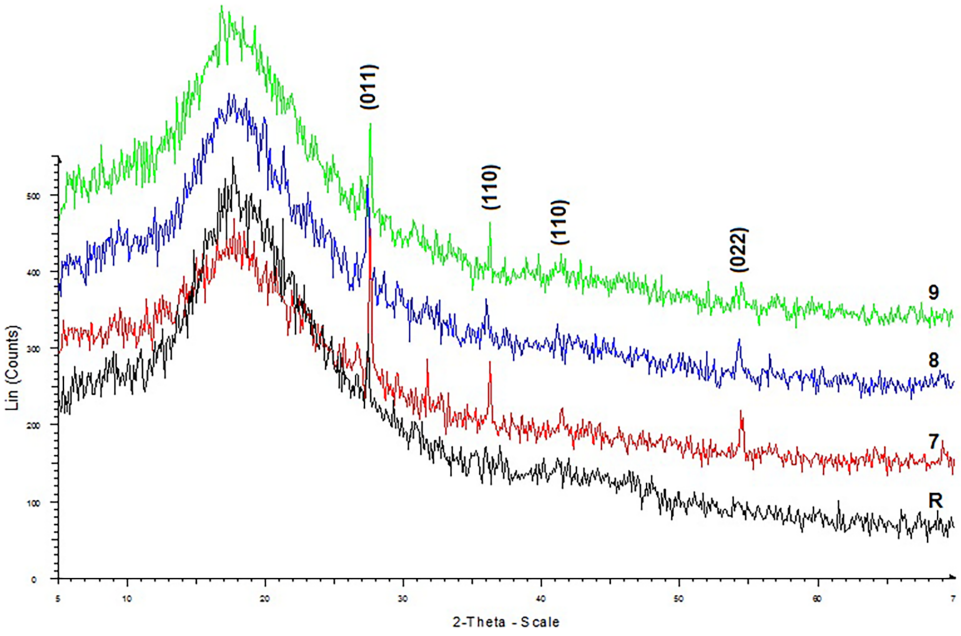

(**c**)

Figure 3: XRD spectra for GFRP samples exposed to different temperatures: (**a**) 20°C; (**b**) 40°C; (**c**) 60°C.

With increasing exposure temperature (20°C–60°C) and immersion time, a progressive decrease in peak intensity and broadening of the amorphous halo can be observed, indicating an increase in structural disorder within the composite. The calculated crystallinity (X_C) values (Table 2) decrease from 20.49% for the reference sample to 15.05% for the most degraded specimen, confirming the influence of saline aging on the internal structure of the material. These are similar to those obtained on different GFRP samples in previous works [7,51,55–57] and indicates the amorphous, sometimes semi-crystalline nature of the analyzed GFRP samples. The crystallinity values calculated from the X-ray spectra indicate a decreasing trend with increasing temperature and exposure time of the materials to the aggressive saline environment. These results are supported by those obtained from the mechanical tests.

The XRD patterns were quantitatively analyzed using Topas 4.1 software through the Rietveld refinement method over the 2θ range of 5°–70°. The amorphous contributions of the epoxy matrix and glass fibers were modeled using calibrated halo functions, while crystalline phases were fitted using pseudo-Voigt profiles. The refinement quality was assessed using weighted profile factors (Rwp < 10%), indicating a reliable fit for the complex composite structure. To evaluate reproducibility, selected samples were analyzed in triplicate, and the variation in relative crystallinity (RC) values was within ±2%–3%.

The observed decrease in RC and the broadening of diffraction features should not be interpreted as a direct cause of mechanical degradation, but rather as structural indicators of progressive hydrothermal aging. In epoxy-based GFRP systems, the tensile performance is primarily governed by fiber integrity, fiber–matrix interfacial bonding, and matrix properties. The diffusion of Na^+ and Cl^- ions, accelerated at higher temperatures (especially 60°C), leads to plasticization of the epoxy network, increasing chain mobility and reducing stiffness. Simultaneously, hydrolysis and degradation of silane coupling agents weaken the fiber–matrix interface, resulting in reduced load transfer efficiency [52,53,58–60].

Table 2: Degree of crystallinity of GFRP samples.

Sample	$X_{C,XRD}$ [%]	Decrease of X_C [%]	Cry Size [nm]	Error	R-Values		
					Rexp, Rwp	GOF (χ^2)	DW
R	20.49	0	12.41	0.92	Rexp: 7.07 Rwp: 7.19	1.02	1.94
1	18.91	7.71	14.22	0.64	Rexp: 7.44 Rwp: 8.08	1.08	1.84
2	18.32	10.59	8.06	0.71	Rexp: 7.51 Rwp: 8.19	1.09	2.00
3	17.65	13.86	5.07	0.81	Rexp: 7.55 Rwp: 8.02	1.06	1.98
4	19.29	5.86	9.98	0.57	Rexp: 6.98 Rwp: 7.39	1.05	2.06
5	15.05	26.55	9.82	0.68	Rexp: 8.68 Rwp: 9.17	1.06	2.16
6	18.79	8.30	9.07	0.78	Rexp: 6.13 Rwp: 6.29	1.03	2.04
7	19.05	7.03	9.59	0.82	Rexp: 7.78 Rwp: 9.18	1.05	2.02
8	18.28	10.79	9.19	0.69	Rexp: 7.26 Rwp: 7.37	1.02	2.07
9	17.89	12.69	9.84	0.65	Rexp: 7.20 Rwp: 7.39	1.03	2.17

The broadening of diffraction peaks further indicates the development of micro-strains and internal stresses within the composite structure, consistent with standard interpretations of XRD peak broadening [52,53,58–60]. In saline environments, these effects can be associated with ion ingress and localized swelling phenomena, as well as the formation of salt deposits within microvoids and interfacial regions, contributing to microstructural damage and mechanical weakening [61–63].

A strong correlation between degree of crystallinity and ultimate tensile strength (UTS) is observed (Fig. 4), with a Pearson correlation coefficient of approximately $r \approx 0.9$. However, this relationship should be interpreted as indirect: RC reflects the extent of structural disorder induced by environmental exposure, while the reduction in UTS is primarily controlled by interfacial degradation and matrix plasticization [61–63].

The degree of crystallinity values presented in Fig. 4 were derived from Rietveld refinement and represent volume-averaged structural parameters, as the X-ray beam irradiates an area of several mm^2. Therefore, each data point integrates information from a large number of microstructural regions, providing a statistically representative characterization of the material. Although local variations in fiber distribution or resin-rich areas may occur, the consistency of the diffraction profiles and the low refinement residuals support the robustness of the observed correlation. Consequently, the XRD-derived crystallinity index can be

considered a reliable indicator of the cumulative physico-chemical degradation of GFRP composites under saline aging conditions.

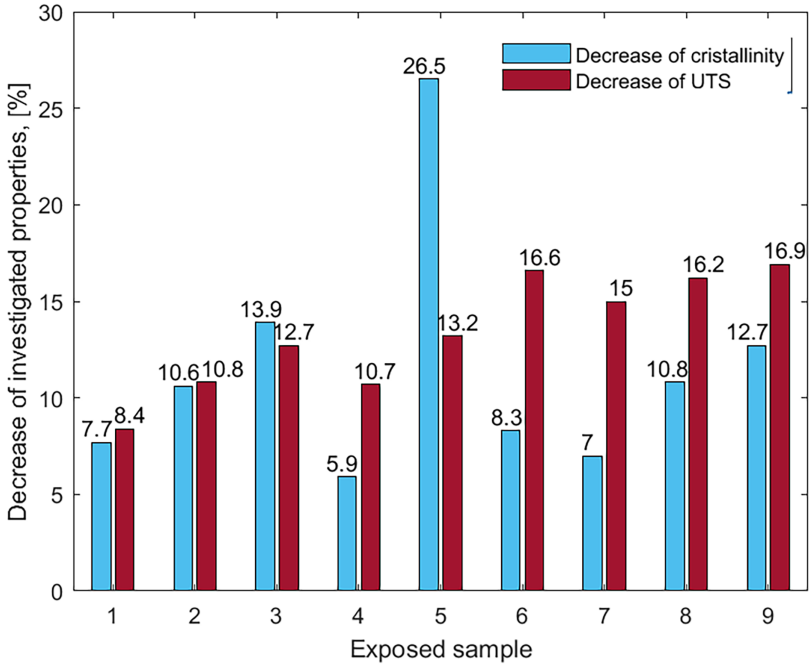

Figure 4: Correlation between degree of crystallinity (X_C) and ultimate tensile strength (UTS) for GFRP composites aged in saline solution at different temperatures. Each XRD data point was derived from Rietveld refinement (R_{WP} < 10%), representing a volume-averaged structural indicator from a scanned surface area of approximately 10\times 10 mm^2.

4.3 Machine Learning Prediction

4.3.1 Ultimate Tensile Strength Prediction Using Machine Learning

To estimate the UTS using machine learning techniques, experimental data obtained from 18 independent tests were utilized. In each experiment, the FRP pipe specimens were subjected to controlled temperature conditions and exposed for different durations to account for time-dependent degradation effects. Each test generated approximately 800 data samples, which were employed for training and validating the machine learning models as well as the classical polynomial regression approach.

In total, 27 independent experiments were conducted, each generating approximately 800 data points corresponding to the stress–strain curve. Given the intrinsic dependence between the points belonging to the same curve, these cannot be considered independent observations. Therefore, to avoid introducing a "data leakage" bias, the dataset was partitioned at the experiment level rather than at the individual data-point level. More specifically, each experiment was entirely allocated to either the training or vali-dation set, thus ensuring a robust and realistic assessment of the performance of machine learning models and polynomial regression.

Fig. 5 illustrates the comparative graphical results obtained using the three machine learning approaches alongside the classical polynomial regression method for each experiment. These plots highlight the ability of the investigated models to approximate the stress–strain behavior. Table 3 summarizes the performance metrics for each method, including R^2, MAE, RMSE, and MSE, as well as the predicted and experimental UTS values for each experimental case, allowing a quantitative comparison of the predictive performance.

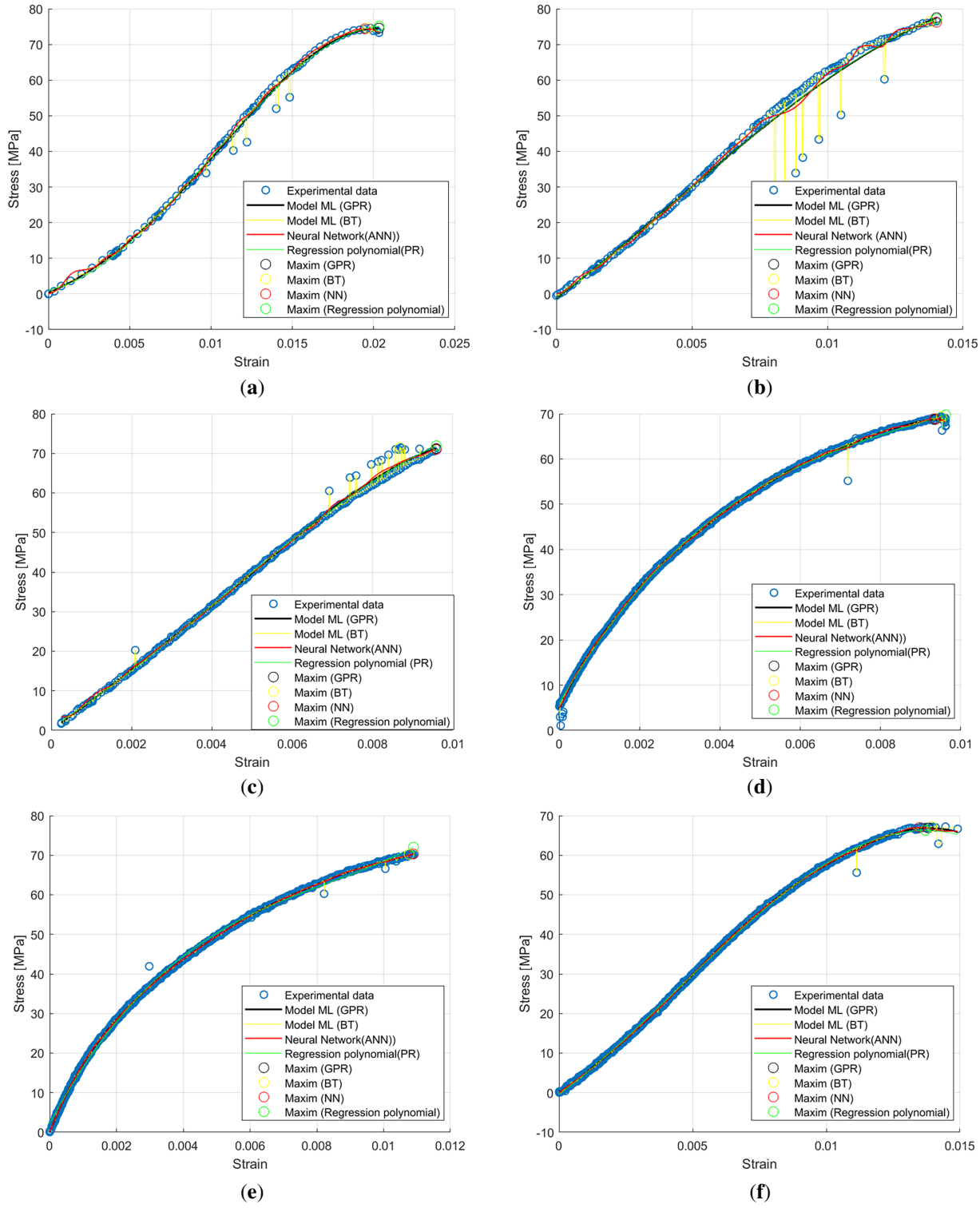

Figure 5: (Continued)

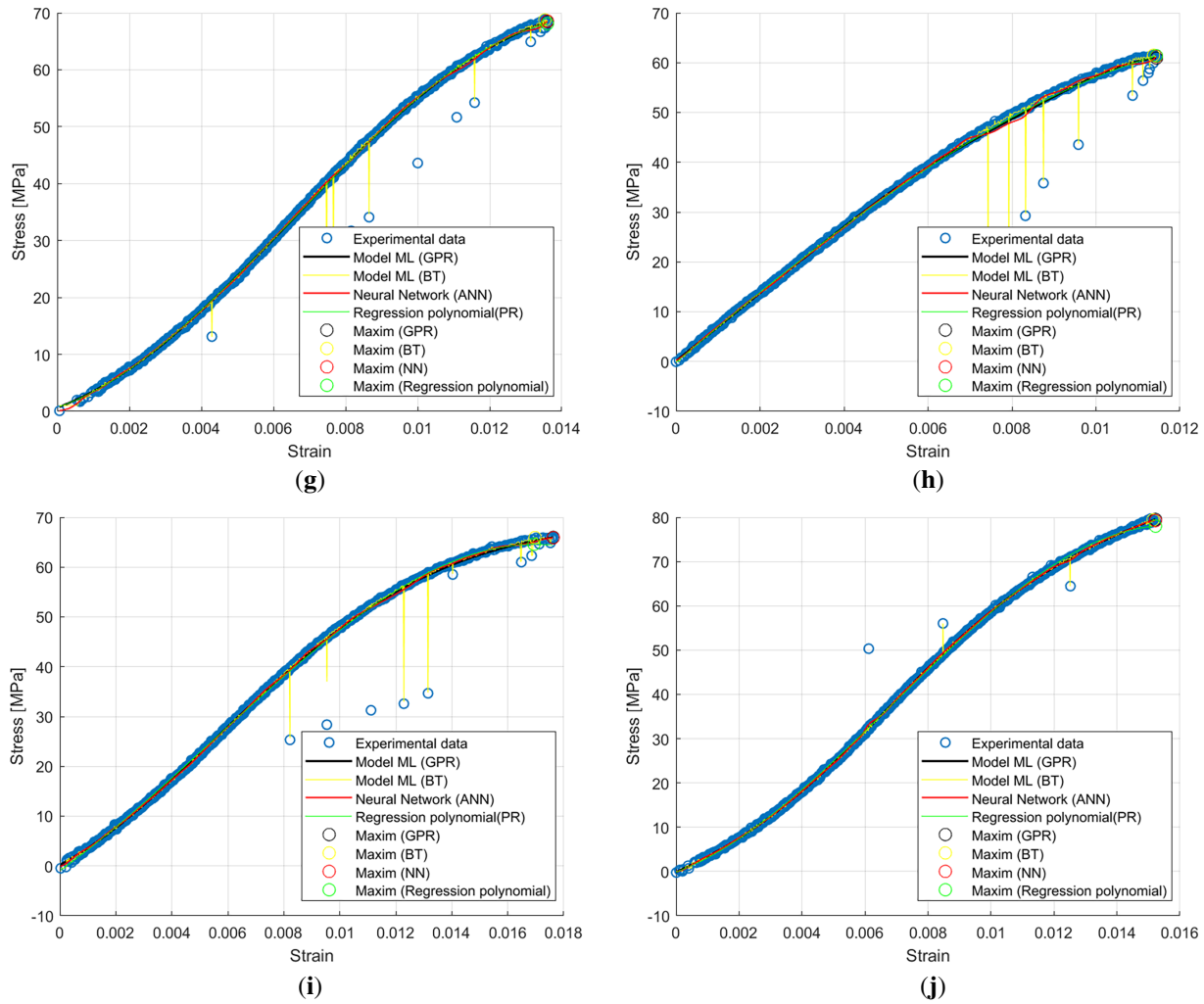

Figure 5: Comparative graphical results using ML and PR for: (**a**) experiment no. 1; (**b**) experiment no. 2; (**c**) experiment no. 3; (**d**) experiment no. 4; (**e**) experiment no. 5; (**f**) experiment no. 6; (**g**) experiment no. 7; (**h**) experiment no. 8; (**i**) experiment no. 9; (**j**) unexposed (reference) sample.

Table 3: Performance metrics for UTS prediction models.

Performance Metrics	R^2	MAE	RMSE	MSE	UTS_Predicted	UTS Experimental	Strain
Experiment No. 1							
EGP	0.99	0.63	2.077	4.31	71.308	71.378	0.01309
BT	0.91	2.44	5.6	31	71.116	71.378	0.0091
ANN	0.98	1.38	2.36	5.61	71.349	71.378	0.01309
PR	0.99	0.96	2.24	5.02	71.129	71.378	0.01309
	Stress(strain) = 1.0e+7 $*$ ($-3.3482 * \text{strain}^3 + 0.0311 * \text{strain}^2 + 0.0007 * \text{strain}$)						

(Continued)

Table 3 (continued)

Performance Metrics	R^2	MAE	RMSE	MSE	UTS_Predicted	UTS Experimental	Strain
Experiment No. 2							
EGP	0.97	1.69	4.25	18.08	74.561	76.54	0.203
BT	0.96	3.20	4.8	23.132	74.579	76.54	0.0196
ANN	0.966	1.41	4.06	16.51	76.53	76.54	0.014
PR	0.967	1.47	4.03	16.25	77.158	76.54	0.014
	Stress(strain) = 1.0e+7 ∗ (−1.385 ∗ strain^3 + 0.0194 ∗ strain^2 + 0.0006 ∗ strain)						
Experiment No. 3							
EGR	0.93	1.524	5.497	30.224	71.209	71.468	0.00959
BT	0.92	2.69	6.20	38.51	71.359	71.468	0.00868
ANN	0.997	0.524	1.081	1.168	71.460	71.468	0.00958
PR	0.997	0.57	1.114	1.242	71.941	71.468	0.0095
	Stress(strain) = 1.0e+7 ∗ (−4.1644 ∗ strain^3 + 0.0516 ∗ strain^2 + 0.0006 ∗ strain)						
Experiment No. 4							
EGP	1	0.32	1.09	1.19	74.521	74.85	0.012
BT	0.99	1.89	2.35	5.53	74.65	74.85	0.012
ANN	0.99	0.32	1.02	1.06	74.87	74.85	0.012
PR	0.99	0.31	1.05	1.102	74.521	74.85	0.012
	Stress(strain) = 1.0e+7 ∗ (−2.1848 ∗ strain^3 + 0.0254 ∗ strain^2 + 0.0006 ∗ strain)						
Experiment No. 5							
EGP	1	0.190	0.35	0.12	70.306	70.246	0.0108
BT	0.99	1.55	1.80	3.25	70. 125	70.246	0.0107
ANN	0.99	0.168	0.292	0.085	70. 235	70.246	0.0108
PR	0.99	0.67	0.804	0.6467	72.048	70.246	0.0108
	Stress(strain) = 1.0e+7 ∗ (6.0219 ∗ strain^3 − 0.150 ∗ strain^2 + 0.0016 ∗ strain)						
Experiment No. 6							
EGP	0.99	0.374	1.487	2.21	65.369	65.59	0.0140
BT	0.99	1.67	2.23	4.99	65. 063	65.59	0.0140
ANN	0,99	0.401	1.44	2.088	65. 564	65.59	0.0140
PR	0.99	0.417	1.44	2.087	64.671	65.59	0.0140
	Stress(strain) = 1.0e+7 ∗ (−1.555 ∗ strain^3 + 0.0160 ∗ strain^2 + 0.005 ∗ strain)						
Experiment No. 7							
EGP	1	0.325	1.206	1.45	68.440	68.842	0.136
BT	0.99	1.73	2.146	4.608	68.069	68.842	0.136
ANN	0.99	0.33	1.135	1.33	68.772	68.842	0.136
PR	0.99	0.32	1.16	1.35	68.069	68.842	0.136
	Stress(strain) = 1.0e+7 ∗ (−3.4077 ∗ strain^3 + 0.067 ∗ strain^2 + 0.0002 ∗ strain)						

(Continued)

Table 3 (continued)

Performance Metrics	R^2	MAE	RMSE	MSE	UTS_Predicted	UTS Experimental	Strain
Experiment No. 8							
EGP	1	0.188	0.33	0.109	65.552	65.699	0.0167
BT	0.99	1.506	1.97	3.88	65.731	65.699	0.0158
ANN	0.99	0.168	0.233	0.054	65.509	65.699	0.0159
PR	0.99	0.69	0.837	0.701	66.984	65.699	0.0156
	Stress(strain) = 1.0e+7 ∗ (−1.5198 ∗ strain^3 − 0.0682 ∗ strain^2 + 0.0072 ∗ strain)						
Experiment No. 9							
EGP	0.99	0.409	1.729	2.991	65.975	65.85	0.0176
BT	0.97	1.87	3.34	11.17	65.922	65.85	0.0169
ANN	0.99	0.417	1.579	2.494	65.966	65.85	0.0169
PR	0.99	0.51	1.63	2.66	64.578	65.85	0.0169
	Stress(strain) = 1.0e+7 ∗ (−1.2951 ∗ strain^3 + 0.0210 ∗ strain^2 + 0.0004 ∗ strain)						
Reference sample							
EGP	1	0.23	0.77	0.607	79.524	79.676	0.0105
BT	0.99	1.751	2.132	4.54	79.396	79.676	0.0151
ANN	0.99	0.23	0.707	0.500	79.455	79.676	0.0152
PR	0.99	0.38	0.81	0.656	77.986	79.676	0.0152
	Stress(strain) = 1.0e+7 ∗ (3.0554 ∗ strain^3 + 0.0630 ∗ strain^2 + 0.0003 ∗ strain)						

An analysis of the performance metrics reported in Table 3 indicates that the Artificial Neural Network (ANN) model generally provides the most accurate approximation of the stress–strain response across the investigated experiments. This observation is supported by the consistently high values of the coefficient of determination (R^2), together with relatively low error indicators (MAE, RMSE, and MSE), in comparison with Exponential Gaussian Process Regression (EGPR), Boosted Trees (BT), and classical polynomial regression (PR).

However, it should be noted that the very high R^2 values (close to 1.0) observed for all models are influenced by the smooth and deterministic nature of the stress–strain curves, which are inherently easier to approximate. Therefore, these results should not be interpreted as evidence of strong generalization capability, but rather as an indication of the models' ability to accurately fit the available experimental data.

In this context, the machine learning models, including ANN, demonstrate strong interpolation capabilities within the range of the available experiments. The predicted UTS values show good agreement with the experimental measurements, further supporting the consistency of the obtained results.

Nevertheless, given the relatively limited number of independent experiments, the proposed ML approach should be regarded as a comparative and exploratory tool rather than a fully generalizable predictive framework.

4.3.2 UTS Estimation as a Function of Operating Conditions

Temperature and exposure time (days) are identified as the primary operating factors affecting the UTS. A two-dimensional interpolation method is employed to estimate the yield stress by capturing the combined influence of these operating conditions.

A two-dimensional interpolation method consists of organizing the experimental data in the form of a matrix, as presented in Table 4, where the first column contains the numerical values of the exposure time (days) and the first row contains the numerical values of temperature. The remaining elements of the matrix represent the ultimate tensile stress (UTS, MPa) values associated with each temperature–time pair.

Table 4: Matrix used for UTS calculation.

	Temperature [°C]		
Expose Time [Day]	**20**	**40**	**60**
30	72.975	71.1	67.68
45	71.065	69.12	66.725
60	69.485	66.395	66.2

For the numerical estimation of UTS (MPa), the authors employed a two-dimensional interpolation technique as a computational tool, which estimates the numerical value of UTS as a discrete function $F(x_1, x_2)$, expressed by an equation of the form

$$UTP(x_1, x_2) = a_0 + a_1 \cdot x_1 + a_2 \cdot x_2 + a_3 \cdot x_1 \cdot x_2 \tag{7}$$

where x_1—exposure time (days) and x_2—temperature.

The implementation of this two-dimensional interpolation method in MATLAB® was carried out by the authors using the gridded Interpolant function. This function returns the interpolated values of the variable Z corresponding to the queried pairs (X_1, Y_1).

Table 5 reports the numerically estimated UTS values corresponding to different combinations of temperature and exposure time (number of days).

Table 5: Numerically estimated UTS values for different combinations of temperature and exposure time.

	Temperature [°C]					
Expose Time [Days]	**20**	**30**	**40**	**50**	**60**	**70**
30	72.975	72.136	71.1	69.42	67.68	66.4179
35	72.404	71.551	70.521	68.9575	67.3434	66.1209
45	71.065	70.095	69.12	67.903	66.725	65.7627
50	70.506	69.272	68.1922	67.3162	66.5357	65.6862
60	69.485	67.795	66.395	66.215	66.2	65.4520
70	68.45	67.020	64.93	65.4890	65.236	64.6740

This trend is further substantiated in Fig. 6 through contour (level-curve) plots, which consistently demonstrate the progressive reduction of the UTS across the parameter space defined by temperature and exposure time.

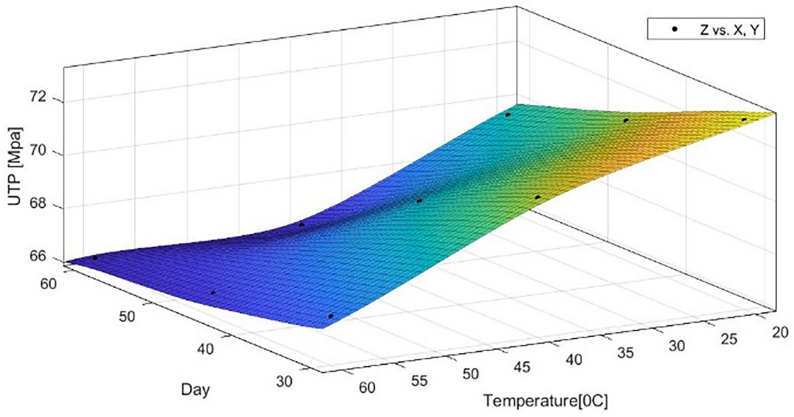

Figure 6: Three-dimensional representation of the two-dimensional interpolation function.

By analyzing the data presented in Table 5, it can be observed that the numerical UTS values are identical to those reported in Table 3 for the same numerical pairs of exposure time (day) and temperature. This agreement demonstrates the correctness and reliability of the two-dimensional interpolation method for the numerical estimation of UTS.

Fig. 7 presents the three-dimensional surface representation of the function defined in Eq. (7), which reveals a pronounced decreasing trend in UTS values with increasing temperature and exposure duration.

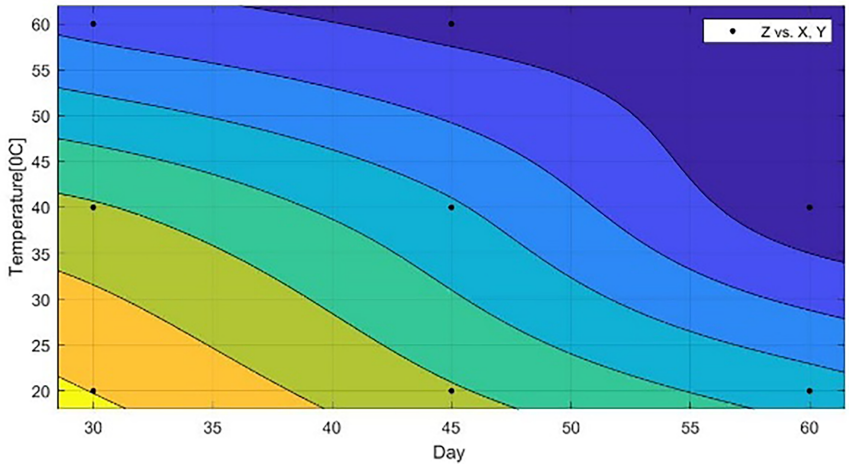

Figure 7: Graphical representation of contour curves associated with function (7).

5 Conclusion

This study provides a comprehensive assessment of the effects of saline environmental exposure on the mechanical and structural stability of glass-fiber-reinforced polymer pipes. These findings confirm that saltwater aging (especially at higher temperatures) degrades the polymer structure of GFRP pipes, reducing crystallinity and UTS. The experimental regression model is strong ($R^2 \approx 0.94$), and our ML models

(particularly Gaussian Process and ANN) can accurately capture the UTS trends (all $R^2 \approx 0.99$ on validation data). Thus, ML-based models, trained carefully with sufficient validation, show promise for predicting FRP performance under realistic environmental aging.

The results demonstrate that although aggressive environments can influence the internal structure of the polymer matrix and gradually reduce mechanical performance, the investigated composite material maintains a relatively stable structural response under the tested conditions. These findings confirm the suitability of GFRP pipes for applications where corrosion resistance and long-term durability are critical requirements.

The microstructural analysis highlighted that environmental exposure induces modifications in the internal organization of the polymer matrix, which are associated with the observed mechanical degradation. Such structural changes indicate that hydrothermal aging processes play a key role in influencing the long-term behavior of composite materials used in pipeline systems.

Another important outcome of this research is the demonstration that data-driven modeling approaches can successfully support the prediction of mechanical performance under varying environmental conditions. The application of machine learning techniques showed that predictive models can capture the complex relationships between environmental factors and material response, offering a valuable tool for performance estimation and durability assessment.

The superior performance of ANN highlights its ability to effectively capture the complex nonlinear relationships between the operating parameters and the mechanical response of the FRP pipes, making it the most reliable estimation technique among those considered in this study.

The results obtained from the two-dimensional interpolation analysis clearly indicate that both temperature and exposure time have a significant influence on the degradation of UTSof FRP pipes. The consistent decreasing trends observed in both the three-dimensional surface plot and the contour representations confirm the progressive reduction of mechanical resistance under more severe operating conditions. These findings highlight the suitability of the proposed interpolation-based approach for capturing the combined effects of thermal and time-dependent factors on material performance, providing a reliable tool for the predictive assessment of structural integrity and long-term durability of FRP piping systems.

It should be noted that the present study is limited by the relatively small number of experimental specimens per condition, which may influence the statistical robustness of the findings. Future investigations involving larger datasets and additional validation are recommended to further confirm the reliability and generalizability of the proposed models.

Acknowledgement: Not applicable.

Funding Statement: The authors received no specific funding for this study.

Author Contributions: The authors confirm contribution to the paper as follows: Conceptualization, Cristina Roxana Popa, Maria Tănase, Gheorghe Brănoiu, Elena-Emilia Sirbu and Cătălina Călin; methodology, Cristina Roxana Popa, Maria Tănase, Gheorghe Brănoiu, Elena-Emilia Sirbu and Cătălina Călin; software, Cristina Roxana Popa, Maria Tănase and Gheorghe Brănoiu; validation, Cristina Roxana Popa and Maria Tănase; formal analysis, Maria Tănase; investigation, Cristina Roxana Popa, Maria Tănase, Gheorghe Brănoiu, Elena-Emilia Sirbu and Cătălina Călin; resources, Maria Tănase; data curation, Cristina Roxana Popa, Maria Tănase, Gheorghe Brănoiu, Elena-Emilia Sirbu and Cătălina Călin; writing—original draft preparation, Cristina Roxana Popa, Maria Tănase, Gheorghe Brănoiu, Elena-Emilia Sirbu and Cătălina Călin; writing—review and editing, Cristina Roxana Popa, Maria Tănase, Gheorghe Brănoiu, Elena-Emilia Sirbu and Cătălina Călin; visualization, Maria Tănase; supervision, Maria Tănase; project administration, Maria Tănase;

funding acquisition, Cristina Roxana Popa, Maria Tănase, Gheorghe Brănoiu, Elena-Emilia Sirbu and Cătălina Călin. All authors reviewed and approved the final version of the manuscript.

Availability of Data and Materials: The datasets analyzed during the current study are available from the corresponding author on reasonable request.

Ethics Approval: Not applicable.

Conflicts of Interest: The authors declare no conflicts of interest.

References

1. Wijewickrama L, Jeewantha J, Perera GIP, Alajarmeh O, Epaarachchi J. Fiber-reinforced composites used in the manufacture of marine decks: a review. Polymers. 2025;17(17):2345. doi:10.3390/polym17172345.
2. Tănase M, Veres C. Green composites in additive manufacturing: a combined review and bibliometric exploration. J Manuf Mater Process. 2025;9(9):301. doi:10.3390/jmmp9090301.
3. Veres C, Tănase M. A bibliometric and systematic review of the use of recycled composite materials with an emphasis on the mechanical performance of structures. Materials. 2025;18(3):607. doi:10.3390/ma18030607.
4. Kennedy SM, Jeen Robert RB, Malkiya Rasalin Prince R, Hikku GS, Kaliraj M. A comprehensive overview of the fabrication and testing methods of FRP composite pipes. MethodsX. 2024;13(34):102990. doi:10.1016/j.mex.2024.102990.
5. De B, Bera M, Bhattacharjee D, Ray BC, Mukherjee S. A comprehensive review on fiber-reinforced polymer composites: raw materials to applications, recycling, and waste management. Prog Mater Sci. 2024;146(2):101326. doi:10.1016/j.pmatsci.2024.101326.
6. Tănase M, Diniță A, Lvov G, Portoacă AI. Experimental determination of circumferential mechanical properties of GFRP pipes using the split-disk method: evaluating the impact of aggressive environments. Appl Sci. 2024;14(24):11845. doi:10.3390/app142411845.
7. Călin C, Diniță A, Brănoiu G, Popovici DR, Tănase M, Sirbu EE, et al. Assessment of environmental impact on glass-fiber-reinforced polymer pipes mechanical and thermal properties. Polymers. 2024;16(13):1779. doi:10.3390/polym16131779.
8. Wang B, Ci S, Zhou M, Di C, Yu J, Zhu B, et al. Effects of hygrothermal and salt mist ageing on the properties of epoxy resins and their composites. Polymers. 2023;15(3):725. doi:10.3390/polym15030725.
9. Uthaman A, Xian G, Thomas S, Wang Y, Zheng Q, Liu X. Durability of an epoxy resin and its carbon fiber-reinforced polymer composite upon immersion in water, acidic, and alkaline solutions. Polymers. 2020;12(3):614. doi:10.3390/polym12030614.
10. Liu X, Wang B, Su Q, Zuo Q, Song X. The long-term interfacial evolution and prediction of carbon- and glass-fiber-reinforced epoxy hybrid rods under a hygrothermal environment. Polymers. 2023;15(10):2278. doi:10.3390/polym15102278.
11. Stamenović M, Putić S, Rakin M, Medjo B, Čikara D. Effect of alkaline and acidic solutions on the tensile properties of glass-polyester pipes. Mater Des. 2011;32(4):2456–61. doi:10.1016/j.matdes.2010.11.023.
12. Robert M, Benmokrane B. Combined effects of saline solution and moist concrete on long-term durability of GFRP reinforcing bars. Constr Build Mater. 2013;38(4):274–84. doi:10.1016/j.conbuildmat.2012.08.021.
13. Miyano Y, Nakada M, Sekine N. Accelerated testing for long-term durability of FRP laminates for marine use. J Compos Mater. 2005;39(1):5–20. doi:10.1177/0021998305046430.
14. Zeng JJ, Zhuge Y, Liang SD, Bai YL, Liao J, Zhang L. Durability assessment of PEN/PET FRP composites based on accelerated aging in alkaline solution/seawater with different temperatures. Constr Build Mater. 2022;327(4):126992. doi:10.1016/j.conbuildmat.2022.126992.
15. Li W, Wen F, Zhou M, Liu F, Jiao Y, Wu Q, et al. Assessment and prediction model of GFRP bars' durability performance in seawater environment. Buildings. 2022;12(2):127. doi:10.3390/buildings12020127.

16. Liao D, Gu T, Liu J, Chen S, Zhao F, Len S, et al. Degradation behavior and ageing mechanism of E-glass fiber reinforced epoxy resin composite pipes under accelerated thermal ageing conditions. Compos Part B Eng. 2024;270:111131. doi:10.1016/j.compositesb.2023.111131.
17. Mazzuca P, Firmo JP, Correia JR, Castilho E. Influence of elevated temperatures on the mechanical properties of glass fibre reinforced polymer laminates produced by vacuum infusion. Constr Build Mater. 2022;345(4):128340. doi:10.1016/j.conbuildmat.2022.128340.
18. dos Santos JC, Siqueira RL, Vieira LMG, Santos Freire RT, Mano V, Panzera TH. Effects of sodium carbonate on the performance of epoxy and polyester coir-reinforced composites. Polym Test. 2018;67:533–44. doi:10.1016/j.polymertesting.2018.03.043.
19. Frigione M, Rodríguez-Prieto A. Can accelerated aging procedures predict the long term behavior of polymers exposed to different environments? Polymers. 2021;13(16):2688. doi:10.3390/polym13162688.
20. Silva MAG, da Fonseca BS, Biscaia H. On estimates of durability of FRP based on accelerated tests. Compos Struct. 2014;116(2):377–87. doi:10.1016/j.compstruct.2014.05.022.
21. Sunny J, Nazaripoor H, Palacios Moreno J, Mertiny P. Accelerated zero-stress hydrothermal aging of dry E-glass fibers and service life prediction using Arrhenius model. Fibers. 2023;11(8):70. doi:10.3390/fib11080070.
22. Tu J, Xie H, Gao K, Li Z, Zhang J. Durability prediction of GFRP rebar based on elastic modulus degradation. Front Mater. 2019;6:258. doi:10.3389/fmats.2019.00258.
23. Tu J, Xie H, Gao K. Prediction of the long-term performance and durability of GFRP bars under the combined effect of a sustained load and severe environments. Materials. 2020;13(10):2341. doi:10.3390/ma13102341.
24. Karbhari VM, Abanilla MA. Design factors, reliability, and durability prediction of wet layup carbon/epoxy used in external strengthening. Compos Part B Eng. 2007;38(1):10–23. doi:10.1016/j.compositesb.2006.06.001.
25. Alsuhaibani E, Yazdani N, Beneberu E. Durability and long-term performance prediction of carbon fiber reinforced polymer laminates. Polymers. 2022;14(15):3207. doi:10.3390/polym14153207.
26. Calabrese L, Fiore V. A simplified predictive approach to assess the mechanical behavior of pinned hybrid composites aged in salt-fog environment. Compos Struct. 2020;249:112589. doi:10.1016/j.compstruct.2020.112589.
27. Shi B, Deng Z. Durability prediction of FRP composite materials under hygrothermal environment. J Phys Conf Ser. 2021;2021(1):012006. doi:10.1088/1742-6596/2021/1/012006.
28. Gupta AK, Zafar S, Pathak H. Mechanical durability of marine-grade glass fiber-reinforced polymer composites exposed to accelerated hygrothermal aging in seawater. J Compos Mater. 2025. doi:10.1177/00219983251391882.
29. Iftikhar A, Manalo A, Senselova Z, Ferdous W, Peerzada M, Seligmann H, et al. Hygrothermal durability and damage evolution of bio-epoxy-based composites reinforced with different fibre types. Polymers. 2026;18(1):58. doi:10.3390/polym18010058.
30. Diniţă A, Rosca CM, Tănase M, Stancu A. A comprehensive review on bridging the research gap in AI-driven material simulation for FRP composites. Comput Model Eng Sci. 2025;144(1):147. doi:10.32604/cmes.2025.066276.
31. Alhusban M, Alhusban M, Alkhawaldeh AA. The efficiency of using machine learning techniques in fiber-reinforced-polymer applications in structural engineering. Sustainability. 2024;16(1):11. doi:10.3390/su16010011.
32. Avevor J, Adeniyi M, Enyejo LA, Aikins SA. Machine learning-driven predictive modeling for FRP strengthened structural elements: a review of AI-based damage detection, fatigue prediction, and structural health monitoring. Int J Sci Res Mod Technol. 2024;3(8):1–20. doi:10.38124/ijsrmt.v3i8.420.
33. Machello C, Rahmati M, Bazli M, Rajabipour A, Arashpour M, Hassanli R, et al. Machine learning-based prediction of bond performance of FRP composite bars in concrete for marine composite structures. Compos Struct. 2025;370(3):119401. doi:10.1016/j.compstruct.2025.119401.
34. Hasan T, Pereira P, Matos JP, Correia JR, Garrido M, Cabral-Fonseca S. Degradation of mechanical properties of FRP composites under hygrothermal exposure: predictive modelling using machine learning tools. In: Proceedings of the 12th International Conference on FRP Composites in Civil Engineering (CICE 2025); 2025 Jul 14–16; Lisbon, Portugal. p. 1915–24. doi:10.1007/978-3-032-09399-8_182.
35. Karimi S, Yu J. Utilizing a combination of experimental and machine learning methods to predict and correlate between accelerated and natural aging of CFRP/AL adhesive joints under hygrothermal conditions. Polym Compos. 2025;46(5):4096–111. doi:10.1002/pc.29226.

36. Ren Y, Wang H. Machine learning-based prediction of long-term durability of FRP and FRP-reinforced concrete: a state-of-the-art review. J Build Eng. 2025;115(1):114482. doi:10.1016/j.jobe.2025.114482.
37. Russell S, Norvig P. Artificial intelligence: a modern approach. London, UK: Pearson; 2020. 1115 p.
38. Bishop CM, Nasrabadi NM. Pattern recognition and machine learning. New York, NY, USA: Springer; 2006. 738 p.
39. Goodfellow I, Bengio Y, Courville A. Deep learning. Cambridge, MA, USA: MIT press; 2017.
40. Hastie T, Tibshirani R, Friedman JH. The elements of statistical learning: data mining, inference, and prediction. Berlin/Heidelberg, Germany: Springer; 2001. 560 p.
41. Popan A, Popan IA, Cosma C, Ceclan V, Balc N. Experimental study on 3D printed parts made of continuous fiberglass reinforced polymer. Acta Tech Napoc Ser Appl Math Mech Eng. 2021;64(1):81–6.
42. Géron A. Hands-on machine learning with Scikit-Learn, Keras, and TensorFlow. Santa Rosa, CA, USA: O'Reilly Media, Inc.; 2022.
43. Sen PC, Hajra M, Ghosh M. Supervised classification algorithms in machine learning: a survey and review. In: Emerging technology in modelling and graphics. Singapore, Singapore: Springer; 2019. p. 99–111. doi:10.1007/978-981-13-7403-6_11.
44. Han J, Kamber M, Pei J. Data mining: concepts and techniques. Amsterdam, The Netherlands: Elsevier; 2011. 740 p.
45. Ang JY, Abdul Majid MS, Mohd Nor A, Yaacob S, Ridzuan MJM. First-ply failure prediction of glass/epoxy composite pipes using an artificial neural network model. Compos Struct. 2018;200:579–88. doi:10.1016/j.compstruct.2018.05.139.
46. Mishra A, Morisetty R. Determination of the Ultimate Tensile Strength (UTS) of friction stir welded similar AA6061 joints by using supervised machine learning based algorithms. Manuf Lett. 2022;32:83–6. doi:10.1016/j.mfglet.2022.04.003.
47. Verma S, Misra JP, Singh J, Batra U, Kumar Y. Prediction of tensile behavior of FS welded AA7039 using machine learning. Mater Today Commun. 2021;26:101933. doi:10.1016/j.mtcomm.2020.101933.
48. Popa C. Tehnici de modelare şi simulare. Ploieşti, Romania: Editura Universităţii Petrol-Gaze Ploieşti; 2020. (In Romanian).
49. Williams CKI. Prediction with gaussian processes: from linear regression to linear prediction and beyond. In: Jordan MI, editor. Learning in graphical models. Dordrecht, The Netherlands: Springer; 1998. p. 599–621. doi:10.1007/978-94-011-5014-9_23.
50. Friedman JH. Greedy function approximation: a gradient boosting machine. Ann Stat. 2001;29(5):1189–232.
51. Allen KA, Kearney LT, Gupta S, Ghossein H, Keum JK, Damron JT, et al. Understanding interfacial crystallization dynamics on carbon fiber reinforced polypropylene composite manufacturing. Compos Part B Eng. 2025;291:112027. doi:10.1016/j.compositesb.2024.112027.
52. Beura S, Chakraverty AP, Pati SN, Pradhan DD, Thatoi DN, Mohanty UK. Effect of salinity and strain rate on sea water aged GFRP composite for marine applications. Mater Today Commun. 2023;34:105056. doi:10.1016/j.mtcomm.2022.105056.
53. Zhang X, Deng Z. Effects of seawater environment on the degradation of GFRP composites by molecular dynamics method. Polymers. 2022;14(14):2804. doi:10.3390/polym14142804.
54. Hamzat AK, Murad MS, Adediran IA, Asmatulu E, Asmatulu R. Fiber-reinforced composites for aerospace, energy, and marine applications: an insight into failure mechanisms under chemical, thermal, oxidative, and mechanical load conditions. Adv Compos Hybrid Mater. 2025;8(1):152. doi:10.1007/s42114-024-01192-y.
55. Hao Y, Liu F, Shi H, Han E, Wang Z. The influence of ultra-fine glass fibers on the mechanical and anticorrosion properties of epoxy coatings. Prog Org Coat. 2011;71(2):188–97. doi:10.1016/j.porgcoat.2011.02.012.
56. Frihi D, Layachi A, Gherib S, Stoclet G, Masenelli-Varlot K, Satha H, et al. Crystallization of glass-fiber-reinforced polyamide 66 composites: influence of glass-fiber content and cooling rate. Compos Sci Technol. 2016;130:70–7. doi:10.1016/j.compscitech.2016.05.007.
57. Rubio Arias JJ, Thielemans W. Efficient depolymerization of glass fiber reinforced PET composites. Polymers. 2022;14(23):5171. doi:10.3390/polym14235171.
58. Zhao Y, Zhang J. Microstrain and grain-size analysis from diffraction peak width and graphical derivation of high-pressure thermomechanics. J Appl Crystallogr. 2008;41(6):1095–108. doi:10.1107/s0021889808031762.

59. Silva MA, Pinho FF, Estêvão MM. Effects of sodium chloride and sulfate on glass fiber-reinforced polymer bars. ACI Mater J. 2018;115(3):401–11. doi:10.14359/51701922.
60. Caceres A, Jamond RM, Hoffard TA, Malvar LJ. Salt-fog accelerated testing of glass fiber reinforced polymer composites. Fort Belvoir, VA, USA: Defense Technical Information Center; 2002. Report No.: TR-2215-SHR.
61. Rudawska A. The effect of the salt water aging on the mechanical properties of epoxy adhesives compounds. Polymers. 2020;12(4):843. doi:10.3390/polym12040843.
62. Gao SL, Mäder E. Characterisation of interphase nanoscale property variations in glass fibre reinforced polypropylene and epoxy resin composites. Compos Part A Appl Sci Manuf. 2002;33(4):559–76. doi:10.1016/S1359-835X(01)00134-8.
63. Zhou J, Lucas JP. The effects of a water environment on anomalous absorption behavior in graphite/epoxy composites. Compos Sci Technol. 1995;53(1):57–64. doi:10.1016/0266-3538(94)00078-6.